Bioinspired soft bendable peristaltic pump exploiting ballooning for high volume throughput

Leone Costi[1], Josephine Hughes[1], *Fumiya Iida[1]

***Abstract*— Interest in bioinspired peristaltic pumps has grown in popularity among the scientific community in the last decade thanks to their extreme flexibility and their intrinsic compliance. In this paper, we propose a soft peristaltic pump exploiting ballooning. Our aim is to promote and propel forward the ballooned region by controlling the air pressure between the balloon and an external flexible containment tube. Thanks to this mechanism, it is possible to achieve a peristaltic pumping motion with a simple design and using only one control signal. In this paper, we describe the implementation of the pump and the inlet-pump-outlet system, provide an analytical model to predict the pump performance, and experimentally test the device. Finally, the proposed pump is directly compared with the state-of-the-art. We show that it is possible to achieve high flow rates, up to $4.5\ \frac{mL}{s}$, with only a single control signal and relying on a much simpler design, paving the way for more flexible and easy to manufacture peristaltic pumps.**

I. INTRODUCTION

Robotics has become integral to everyday life in modern society, but rigid robots show strong limitations in compliance, safety, and flexibility. This is where soft robotics excels, using stretchable and flexible materials as structural elements and actuators [1], [2], [3]. Considering the subdomain of peristaltic pumps, rigid pumps achieve the characteristic peristaltic motion by temporally crimping the tube with rollers [4], potentially cutting and damaging the tube if the medium contains solid particles. Conversely, soft pumps reproduce the peristaltic motion observed in biological systems [5] by understanding and replicating motion primitives observed in nature [6], [7], [8], achieving high compliance and good flexibility. The bending capability of such devices makes them suitable for performing actuation in narrow and tight spaces with obstacles, such as medical applications [9].

The actuation technologies that have been exploited so far for peristaltic actuation are dielectric active elastomers (DAEs) [10], [11], [12], magnetic actuators (MAs), shape memory alloys (SMAs) [13], [14] and pneumatic artificial muscles (PAMs) [15], [16], [17]. Among these, DAEs and MAs are able to achieve high frequencies, up to $10\ Hz$, but the limited stroke is unable to provide high flow rates. Instead, PAMs showcase the best flow rate, around $10\ \frac{mL}{s}$, thanks to a modular architecture bioinspired from the small intestine [18], [19], [20]. Although powerful, this solution shows extreme complexity in fabrication, control, and scalability. The fabrication of each actuator is performed through silicone casting which requires considerable time for manual fabrication. In addition, due to the modular design, each module needs to be connected to the air supply and controlled independently. Overall, state-of-the-art pumps show either a low flow rate or extreme complexity and limited flexibility due to the wiring.

In this work, we propose a non-modular design exploiting and controlling the buckling of an elastomeric balloon, known as ballooning. Ballooning is the phenomenon by which balloons, when inflated, rapidly create a localized completely expanded region, with little deformation of the rest of the structure [21]. Theoretically, the position of the ballooned region along the balloon can be easily changed since all possible positions are energetically equivalent [21], [22]. Our aim is to promote ballooning and then propel the inflated region forward, after which reversing the buckling at the end of the pump to create a peristaltic pumping motion that can then be cycled. However, controlling buckling is a complex and problematic task, since it is an unstable phenomenon very sensitive to any change in geometry or load [23], [24], [25].

We propose using an external flexible tube to constrain the balloon. If the inner diameter of the tube is smaller than the diameter of the inflated balloon, the ballooning would seal the tube and create two distinct regions: one proximal, between the inlet and the inflated region, and the other distal, between inflated region and outlet. By constraining it in this way, we can then use a single control pressure signal on the proximal region to achieve the peristaltic motion, allowing on/off control to trigger pumping. Finally, by developing a mathematical model of the inlet-pump-outlet system, we aim to give an additional tool for designing soft pumps that exploit ballooning.

In the remainder of the paper, we present the pump design and fabrication in Section II-A, followed by the overall setup in Section II-B, the mathematical model in Section II-C, and the experimental design and results in Sections II-D and III.

II. MATERIAL AND METHODS

A. Pump design and fabrication

The proposed pump design consists of two main components: the balloon and the external tube. The balloon is kept in position inside the tube by two supports that also connect the balloon to the inlet and outlet tubes. The left support also provides the connection to the air supply from the pneumatic regulator so that the pressure between balloon and tube can be regulated and controlled (see Fig. 1).

For the fabrication, we used a $2.2 \cdot 10^{-3}\ cm$ thick natural latex balloon (*Pengxiaomei, Modelling Balloons*) [26], [27] and a PET-PVC external tube (*RS Components, 368-0233*)

[1] The Bio-Inspired Robotics Lab, Department of Engineering, University of Cambridge, UK. *fi224@cam.ac.uk.com

[28]. The external tube's length is 45 cm to match the partially inflated balloon's length, and its internal diameter is 0.126 cm to ensure a tight junction with the balloon. The inlet and outlet supports have been 3D printed with ABS to fit the ends of the pump and host the needed connections. All the components are assembled together by hand.

In order to achieve spontaneous ballooning, the device needs to be placed at a lower level than the water source connected to the inlet, so that the fluid pressure inside the balloon can trigger the buckling, and the balloon presents itself with an inflated region. Experimentally has been observed that placing the device at a distance $h = 160\ cm$ below the water source produces a spontaneously inflated region of length $l_p = 20\ cm$. This phenomenon is more likely to happen in the proximal section because of balloons' imperfections.

The control of the pump is open-loop and the control signal used to achieve peristaltic motion is a square pressure wave between balloon and tube, supplied by the pneumatic regulator. The 3 tunable parameters are the maximum pressure P and the activation and rest time, t_{on} and t_{off} respectively (Fig. 2).

The pumping cycle can be divided into four parts: buckling, recoil, inverse buckling, and propulsion (see Fig. 3). Buckling and recoil happen when the pressure between the balloon and the external tube is at the atmospheric level: buckling happens when the pneumatic regulator is switched off, due to the differential pressure between inside and outside the balloon, whereas recoil is the passive flow from inlet to outlet, due to a lack of pressure in the outlet following the ballooning. Conversely, propulsion and inverse buckling happen when the pneumatic regulator is switched on. The buckled balloon divides the external tube is two regions, one proximal and one distal: only the proximal is pressurized since the regulator is connected on the inlet side, resulting in a force propelling the inflated region forward.

B. Setup

Once the pump is assembled, it is connected to the inlet and the outlet tubes, which connect the pump with both source and target. The left support is also connected to the pneumatic regulator, which uses an air compressor operating at 10 bar as a source. The pneumatic regulator is controlled with Arduino UNO to achieve the square pressure wave. The pump is kept at a distance h below the fluid source and the target reservoir. Fig. 4 shows the experimental set-up and a corresponding schematic.

C. Mathematical model

In this section, a mathematical model of the overall system is proposed in order to predict the performance as a function of the square pressure wave's parameters t_{on} and t_{off}. The following demonstration is divided into the four phases of the pumping cycle: buckling, recoil, inverse buckling, and

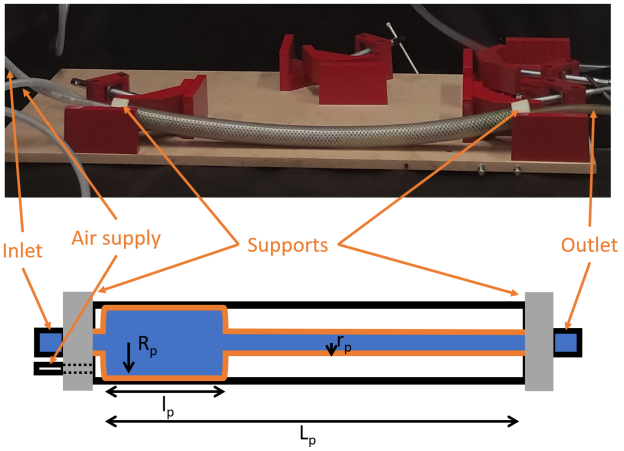

Fig. 1. Experimental pump implementation showing inlet, outlet and air supply. The parameters in figure are $L_p = 45\ cm$, $l_p = 20\ cm$, $R_p = 0.63\ cm$ and $r_p = 0.2\ cm$.

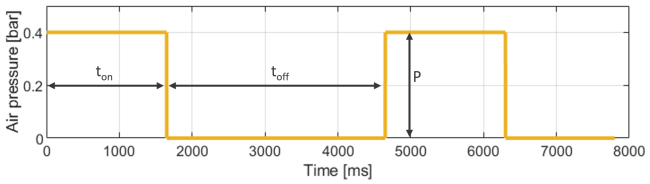

Fig. 2. Control pressure signal used to create peristaltic motions. P is the high pressure value of the square wave, and t_{on} and t_{off} are the activation and rest time, respectively.

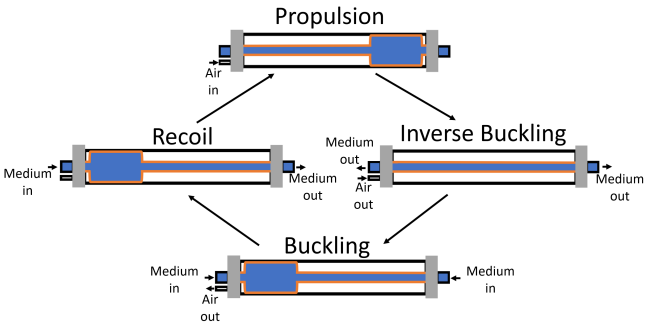

Fig. 3. Schematics of the pumping cycle and its four phases. Propulsion and inverse buckling happen during the activation of the pneumatic regulator, while buckling and recoil happen in the rest time.

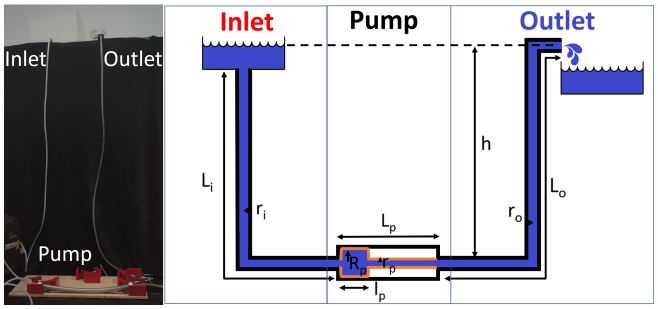

Fig. 4. Implementation and schematics of the set-up used to test the performance of the pump. $L_i = L_o = 300\ cm$, $r_i = r_o = 0.24\ cm$, $h = 160\ cm$, $L_p = 45\ cm$, $l_p = 20\ cm$, $r_p = 0.2\ cm$ and $R_p = 0.63\ cm$.

propulsion. For ease of discussion we will discuss the process in this order, whereas in the real system, propulsion happens before inverse buckling. Since the buckling is a much faster phenomenon than recoil or propulsion of the inflated region, both the buckling and the inverse buckling will be considered instantaneous. All pressure values are referred to as gauge pressure.

1) Buckling: When the regulator switches off, the fluid's pressure $\rho g h$ (where ρ is the density of the inner fluid and g is the gravitational acceleration) causes ballooning, creating an inflated region that is filled with water from both outlet and inlet (see Fig. 5 a and b). Assuming that this phase happens instantly, it is supposed that the volume of water introduced in the pump $V_p = l_p \pi (R_p^2 - r_p^2)$ is provided by inlet and outlet depending on their distance from the middle point of the inflated region:

$$\begin{cases} O_{o1} = V_p \frac{L_{i1}}{L_{i1}+L_{o1}} \\ O_{i1} = V_p \frac{L_{o1}}{L_{i1}+L_{o1}} \end{cases} \tag{1}$$

where O_{o1} and O_{i1} are the volume of fluid provided by the outlet and the inlet, respectively, L_{i1} is the length of the inlet tube plus the distance from the start of the pump until the center of the inflated region and L_{o1} is the length of the outlet tube plus the remaining length of the pump, at this specific phase. The index 1 is used to indicate the first phase: buckling. Then, it is possible to compute the height $d_0 = \frac{O_{o1}}{\pi r_o^2}$, which is the starting point of the recoil.

2) Recoil: The recoil describes how the fluid level of the outlet raises to match the inlet. During this phase the entire system can be schematize as a fluid reservoir with an orifice at a distance d below the level of the fluid (see Fig. 5 c and d). The solution of such a model is known as Torricelli's law, but in our case the distance $d(t)$ is a function of the velocity of the fluid at the orifice, $v(t)$, leading to the following set of equations:

$$\begin{cases} v(t) = \sqrt{2gd(t)} \\ d(t) = d_0 - \int_0^t v(x)\, dx \end{cases} \tag{2}$$

Substituting in and integrating, you can get:

$$v^2(t) = 2g(d_0 - V(t) + V(0)) \tag{3}$$

where $V(t)$ is the anti-derivative of $v(t)$. Finally, by deriving with respect to t we obtain the fluid's acceleration as $\dot{v(t)} = -g$, hence both $v(t)$ and $d(t)$ can be rewritten as:

$$\begin{cases} v(t) = \sqrt{2gd_0} - gt \\ d(t) = d_0 + \frac{g}{2}t^2 - \sqrt{2gd_0}t \end{cases} \tag{4}$$

Finally, we can compute the volume of fluid that is still needed to completely fill the outlet tube at the end of the recoil as $M = \pi r_o^2 d(t_{off})$.

3) Inverse buckling: This phase is the only one in which we have a net positive flow rate going into the receiving container (see Fig. 5 e and f). The total volume of water ejected is:

$$O_{tot} = O_{o3} + O_{reb} \tag{5}$$

where the first term is due to the inverse buckling and the second one is due to the rebound of the balloon itself after.

Following the same assumption of the buckling phase and correcting the outlet volume by the volume M obtained during the recoil phase, it is possible to compute the volume of water ejected by inverse buckling as follows:

$$\begin{cases} O_{o3} = V_p \frac{L_{i3}}{L_{i3}+L_{o3}-d(t_{off})} - M \\ O_{i3} = V_p \frac{L_{o3}-M}{L_{i3}+L_{o3}-d(t_{off})} \end{cases} \tag{6}$$

where V_p is the volume of fluid inside the balloon before buckling, O_{o3} and O_{i3} are the volume of fluid ejected in the outlet's and inlet's reservoirs, respectively, L_{i3} is the length of the inlet tube plus the distance from the start of the pump until the center of the inflated region and L_{o3} is the length of the outlet tube plus the remaining length of the pump, at this specific phase. The index 3 is used to indicate the third phase: inverse buckling. Note that the inverse buckling happens distally, whereas the buckling happens proximally.

The second contribution is due to the rebound of the balloon. When an instantaneous change in volume happens (i.e. inverse buckling), the volume between the balloon and the tube increases suddenly, thus decreasing the pressure. Simultaneously, the air compressor tries to bring the pressure back up while the balloon would start inflating due to the fluid pressure on the inside. Those two phenomena cause a rebound of the balloon and more fluid is ejected as a consequence. Given the complexity of this problem, an analytical formulation is not provided, and the magnitude of the rebound is approximated as a second-order decaying phenomenon with respect to time: $A(t) = (at^2 + bt + c)$. The rebound's contribution O_{reb} can then be computed as follows:

$$O_{reb} = \left(\frac{L_{i3}}{L_{i3} + L_{o3} - d(t_{off})} - M\right) \int_0^t A(x)\, dx \tag{7}$$

The parameters a, b and c are selected using the Nelder-Mead simplex optimization algorithm [29] on the experimental data: $a = -3.9941 \times 10^{-}10\ \frac{mL}{s^3}$, $b = -4.9844 \times 10^{-}7\ \frac{mL}{s^2}$ and $c = 6.6 \times 10^{-}3\ \frac{mL}{s}$.

4) Propulsion: Upon activation of the regulator, the air-flow introduced pushes the inflated region of the balloon from the proximal region to the distal one, where the inverse buckling happens. In the experiments the needed time for this process has been measured to be $\tau = 500\ ms$ for a $0.4\ bar$ air pressure. Taking into consideration this time delay, the average flow rate of the pump F can be predicted as follows:

$$F = \frac{O_{o3}(t_{off})u(t_{on} - \tau) + O_{reb}(t_{on}, t_{off})}{t_{on} + t_{off}} \tag{8}$$

where $u(t)$ is the unit step function.

D. Experiments

When testing the pump, the main outcome considered is the average flow rate: the pump is activated for five cycles and the total volume of water is then divided by the time needed to complete the cycles. All experiments are run using water and every experiment is repeated 6 times with different

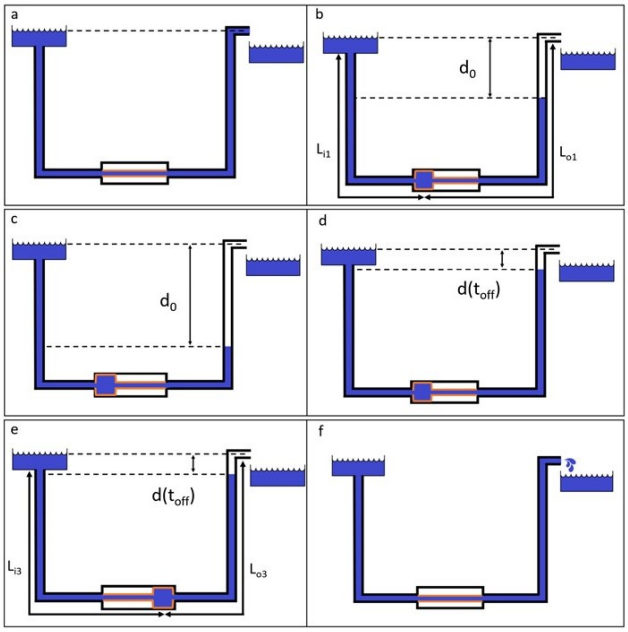

Fig. 5. Schematics of (a) before and (b) after the onset of the inverse buckling, (c) at the beginning and (d) at the end of the recoil, and (e) before and (f) after the onset of the buckling.

balloons. Since the only control signal is a square pressure wave, the only 3 controllable parameters are P, t_{on}, and t_{off}. The parameters are initialized at $0.4\ bar$, $1650\ ms$ and $7000\ ms$, respectively, and are optimized individually: first t_{on}, then t_{off} and lastly P. Next, the pump's performance in 5 configurations of increasing bending radius, up to $360\ deg$, is analyzed. Finally, the pump is also tested using coffee powder to simulate solid particles inside the water.

III. RESULTS

First, keeping $P = 0.4\ bar$ and $t_{off} = 7000\ ms$, the pump has been tested and its performance has been evaluated as a function of t_{on} (Fig. 6 a). Next, fixing $t_{on} = 1650\ ms$, which corresponded to the maximum flow, the performance has been evaluated as a function of t_{off} (see Fig. 6 b). It can be noticed that the best performance is obtained for $t_{on} = 1650\ ms$ and $t_{off} = 3000\ ms$, but the pump is able to achieve a good performance up to a frequency of $1\ Hz$, with $t_{on} = 500\ ms$ and $t_{off} = 500\ ms$. If t_{on} is not enough to trigger the inverse buckling, there is a drop in performance due to the inflated region of the balloon not contributing to the ejected volume. It is also clear that the rest time needs to be sufficient for the fluid recoil to happen, otherwise, the majority of the ejected volume is wasted in the outlet tube and does not contribute to the pump's flow rate. Moreover, the proposed mathematical model is shown to enable accurate prediction of the pumps performance.

Next, keeping constant the optimized parameters $t_{on} = 1650\ ms$ and $t_{off} = 3000\ ms$, the effect of the pressure's amplitude is investigated (see Fig. 7). The bar chart shows that both low and high pressures result in a substantial

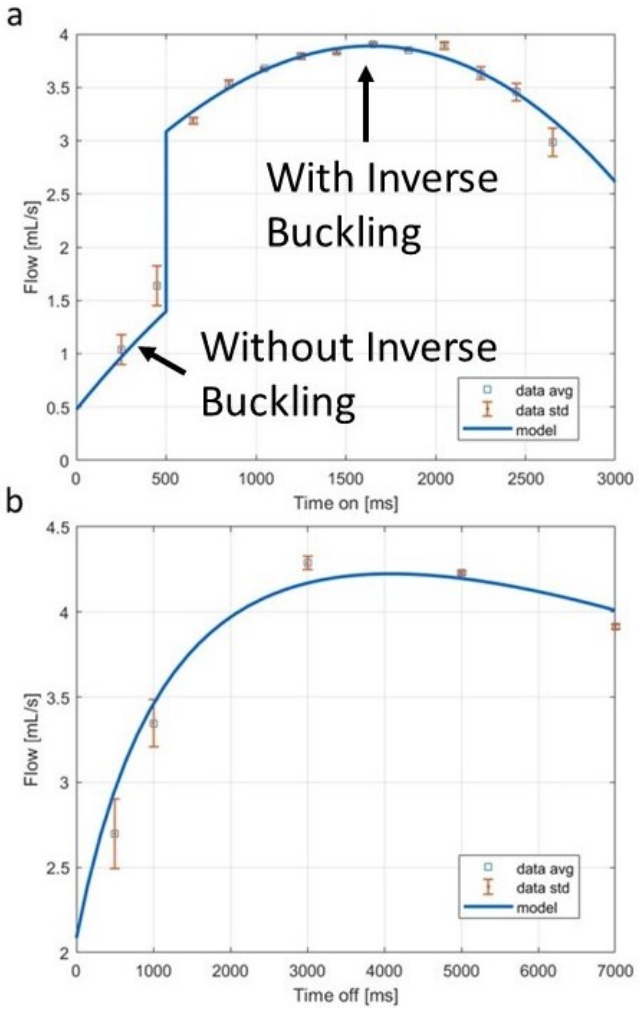

Fig. 6. Performance of the pump as a function of the activation and rest time, respectively. In (a) $t_{off} = 7000\ ms$ and in (b) $t_{on} = 1650\ ms$. Each tested value has been sampled 6 times using 6 different balloons.

decrease in performance. Analytically, increasing the operating pressure results in a lower τ and lower magnitude of the rebound $A(t)$. With a pressure of $0.2\ bar$, the force exerted on the inflated region is not sufficient to propel it forward and to promote the inverse buckling, lowering the total volume of fluid ejected per cycle. On the other hand, high values of pressure ($0.6\ bar$ and $0.8\ bar$) are achieved by increasing the pneumatic regulator's airflow rate, which decreases significantly the magnitude of $A(t)$ (see Eq. 5).

To test the flexibility of the proposed pump design, the best operational parameters $P = 0.4\ bar$, $t_{on} = 1650\ ms$ and $t_{off} = 3000\ ms$ are tested while bending the pump in different configurations. Fig. 8 shows the relative flow rate with respect to the unbent configuration and how the different orientations are achieved. The results show that the effect of bending is limited at most to 11%, thus the pump could be used in clustered and dynamic environments and could be bent around obstacles without extreme losses, making it suited for tasks in narrow spaces with obstacles to avoid, such as surgical theaters and healthcare facilities [31].

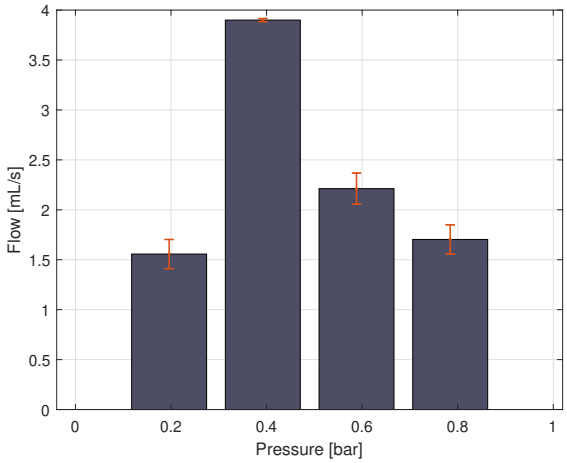

Fig. 7. Performance at different values of applied pressure, with $t_{on} = 1650\ ms$ and $t_{off} = 3000\ ms$. Each tested value has been sampled 6 times using 6 different balloons.

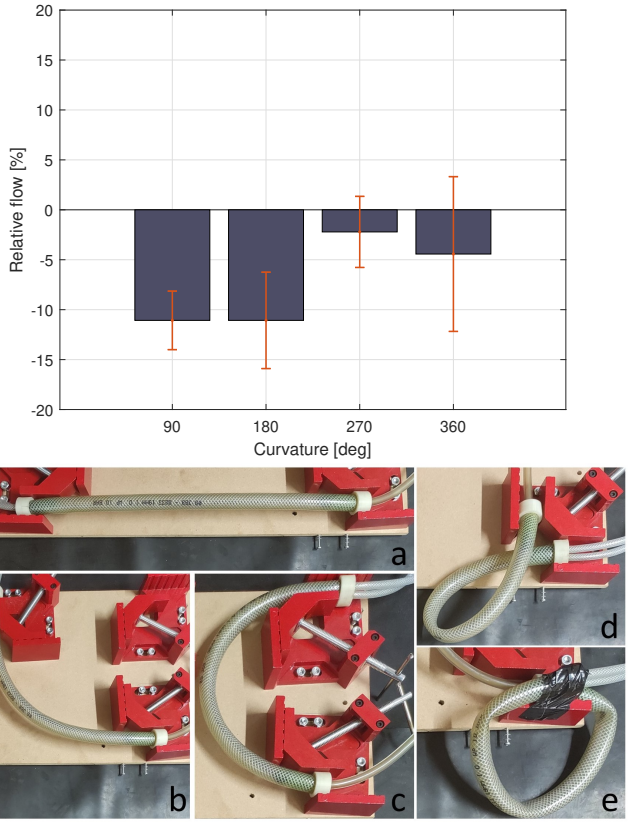

Fig. 8. Relative flow rate with respect to the unbent configuration as the angle between inlet and outlet is increased: (a) 0 deg, (b) 90 deg, (c) 180 deg, (d) 270 deg and (e) 360 deg. Each tested configuration has been sampled 6 times using 6 different balloons.

Finally, to investigate the effect of solid particles in the medium, the device is tested pumping a slurry obtained by mixing 150 g of coffee powder and 4 L of water, with the same optimal parameters. We run the experiments with both water and the mixture, and while pumping the latter the flow rate is only $0.6 \pm 0.2\%$ lower, showing that the presence of the powder does not affect at all the performance.

When compared with other state-of-the-art biomimetic peristaltic soft pumps (see Table I), this proposed solution shows good performance, in particular for the flow rate, which is second only to modular PAMs. In addition, the pump showcases an extremely simple design, fabrication process, and control strategy, with only one control signal required to achieve its high flow rate.

IV. CONCLUSION

This work proposes an innovative strategy to achieve bioinspired peristaltic soft pumping: controlling the spontaneous buckling of a balloon filled with fluid. The pump is composed only of the balloon containing the medium and an external tube, resulting in a simple design and an easy fabrication process. Our pump needs to be placed at a given distance below the level of the source and target reservoirs to trigger the instability, but this constraint could be avoided by promoting the ballooning with a vacuum between the balloon and the external tube. Note that this could be achieved using the same pneumatic line to impose vacuum instead of atmospheric pressure during buckling and recoil, thus not needing a second one. The inflated region is moved using a single pneumatic regulator connected to the proximal end. A mathematical model is introduced to predict the performance of the pump, considering the overall testing bench. The effects of amplitude, activation time, and

TABLE I

OVERVIEW OF BIOMIMETIC PERISTALTIC PUMPING SYSTEM UTILIZING DIFFERENT ACTUATION PRINCIPLES.

Authors	Actuation principle	Inner diameter $[cm]$	Length $[cm]$	Control signals	flow rate $[\frac{mL}{s}]$	Frequency $[Hz]$
Bowers et al.[10]	Dielectric active elastomer	4	0.25	1	0.04	$3-4$
McCoul et al.[11]	Dielectric active elastomer	1.5	5	1	–	–
Lotz[12]	Dielectric active elastomer	0.1	3.5	1	1.8×10^{-4}	10
Fuhrer et al.[30]	Magnetic actuation	0.95	24	4	1.3	4
Miki et al.[13]	Shape memory alloy	1.8	3.5	2	$3-6$	0.33
Sun et al.[14]	Shape memory alloy	0.9	8	3	0.013	$0.1-2$
Suzuki et al.[18]	Pneumatic artificial muscle	3	23.5	5	33	$1.2-2$
Dirven et al.[16]	Pneumatic artificial muscle	1.8	20	12	$5-10$	–
Esser et al.[9]	Pneumatic artificial muscle	2	26.7	8	14	1.25
Our solution	Pneumatic buckling	2	45	1	$3-5$	$0.2-1$

rest time on the flow rate have been analyzed to provide a complete characterization. When compared with state-of-the-art soft peristaltic pumps, our approach is shown to have a high flow rate: much greater than the other single input systems and second only to complex modular designs. Our device maintains high volume throughput until $1\ Hz$ before strongly decreasing its performance, due to failed propulsion and recoil's time scale. Moreover, our design is proven to be much simpler than the current state-of-the-art, given the need for only one control signal, the faster and easier fabrication process, and the scalability of the device. Unlike the other pneumatic solutions in literature, the proposed pump is not modular, thus the length of the pump itself does not affect the fabrication nor the number of control signals needed to operate it. Finally, the extreme versatility of the device is tested by actuating it in various bent configurations and using different media, and the performances are only slightly affected. In summary, utilizing buckling provides many advantages to the pumping mechanism, enabling many novel functionalities and state-of-the-art performance. Future work could include the parallel implementation of different balloons pumping different media and the systematic introduction of weak points to better control and stabilize the buckling.

ACKNOWLEDGMENT

This work was supported by the SMART project, European Union's Horizon 2020 research and innovation under the Marie Sklodowska-Curie (grant agreement ID 860108).

REFERENCES

[1] J. Walker, T. Zidek, C. Harbel, S. Yoon, F. S. Strickland, S. Kumar, and M. Shin, "Soft robotics: A review of recent developments of pneumatic soft actuators," *Actuators*, vol. 9, no. 1, 2020.

[2] D. Ferrero, "Soft touch," *Twist*, no. 5, pp. 40–41, 2009.

[3] S. Kim, C. Laschi, and B. Trimmer, "Soft robotics: A bioinspired evolution in robotics," *Trends in Biotechnology*, vol. 31, no. 5, pp. 287–294, 2013. [Online]. Available: http://dx.doi.org/10.1016/j.tibtech.2013.03.002

[4] J. Klespitz and L. Kovács, "Peristaltic pumps - A review on working and control possibilities," *SAMI 2014 - IEEE 12th International Symposium on Applied Machine Intelligence and Informatics, Proceedings*, pp. 191–194, 2014.

[5] S. Vogel, "Living in a physical world X. Pumping fluids through conduits," *Journal of Biosciences*, vol. 32, no. 2, pp. 207–222, 2007.

[6] C. G. Fontanella, C. Salmaso, I. Toniolo, N. de Cesare, A. Rubini, G. M. De Benedictis, and E. L. Carniel, "Computational Models for the Mechanical Investigation of Stomach Tissues and Structure," *Annals of Biomedical Engineering*, vol. 47, no. 5, pp. 1237–1249, 2019.

[7] D. Liao, D. Lelic, F. Gao, A. M. Drewes, and H. Gregersen, "Biomechanical functional and sensory modelling of the gastrointestinal tract," *Philosophical Transactions of the Royal Society A: Mathematical, Physical and Engineering Sciences*, vol. 366, no. 1879, pp. 3281–3299, 2008.

[8] D. Bach, F. Schmich, T. Masselter, and T. Speck, "A review of selected pumping systems in nature and engineering - Potential biomimetic concepts for improving displacement pumps and pulsation damping," *Bioinspiration and Biomimetics*, vol. 10, no. 5, 2015.

[9] F. Esser, T. Masselter, and T. Speck, "Silent Pumpers: A Comparative Topical Overview of the Peristaltic Pumping Principle in Living Nature, Engineering, and Biomimetics," *Advanced Intelligent Systems*, vol. 1, no. 2, p. 1900009, 2019.

[10] A. E. Bowers, J. M. Rossiter, P. J. Walters, and I. A. Ieropoulos, "Dielectric elastomer pump for artificial organisms," *Electroactive Polymer Actuators and Devices (EAPAD) 2011*, vol. 7976, no. March 2011, p. 797629, 2011.

[11] D. McCoul and Q. Pei, "Tubular dielectric elastomer actuator for active fluidic control," *Smart Materials and Structures*, vol. 24, no. 10, 2015.

[12] P. Lotz, M. Matysek, and H. F. Schlaak, "Peristaltic pump made of dielectric elastomer actuators," *Electroactive Polymer Actuators and Devices (EAPAD) 2009*, vol. 7287, no. April 2009, p. 72872D, 2009.

[13] H. Miki, T. Okuyama, S. Kodaira, Y. Luo, T. Takagi, T. Yambe, and T. Sato, "Artificial-esophagus with peristaltic motion using shape memory alloy," *International Journal of Applied Electromagnetics and Mechanics*, vol. 33, no. 1-2, pp. 705–711, 2010.

[14] X. Sun, Y. Hao, S. Guo, X. Ye, and X. Yan, "The development of a new type of compound peristaltic micropump," *2008 IEEE International Conference on Robotics and Biomimetics, ROBIO 2008*, pp. 698–702, 2009.

[15] F. J. Chen, S. Dirven, W. L. Xu, and X. N. Li, "Soft actuator mimicking human esophageal peristalsis for a swallowing robot," *IEEE/ASME Transactions on Mechatronics*, vol. 19, no. 4, pp. 1300–1308, 2014.

[16] S. Dirven, J. Allen, W. Xu, and L. K. Cheng, "Soft-robotic esophageal swallowing as a clinically-inspired bolus rheometry technique," *Measurement Science and Technology*, vol. 28, no. 3, 2017.

[17] S. Yoshihama, S. Takano, Y. Yamada, T. Nakamura, and K. Kato, "Powder conveyance experiments with peristaltic conveyor using a pneumatic artificial muscle," *IEEE/ASME International Conference on Advanced Intelligent Mechatronics, AIM*, vol. 2016-Septe, pp. 1539–1544, 2016.

[18] T. Nakamura and K. Suzuki, "Development of a peristaltic pump based on bowel peristalsis using artificial rubber muscle," *Advanced Robotics*, vol. 25, no. 3, pp. 371–385, 2011.

[19] M. Firouzi, F. Röhrbein, J. Conradt, C. Richter, G. Dikov, and J. Conradt, *Spiking Cooperative Stereo-Matching at 2 ms Latency with Neuromorphic Hardware*, 2017, vol. 1, no. ii. [Online]. Available: https://www.researchgate.net/publication/318449954

[20] A. Mura, M. Mangan, N. Lepora, T. J. Prescott, P. F. M. J. V. Eds, and R. Goebel, *Living Machines 2018 Proceedings*, 2011.

[21] A. Giudici and J. S. Biggins, "Ballooning, bulging and necking: an exact solution for longitudinal phase separation in elastic systems near a critical point." *arXiv*, pp. 58–61, 2020.

[22] A. Rafsanjani, L. Jin, B. Deng, and K. Bertoldi, "Propagation of pop ups in kirigami shells," *Proceedings of the National Academy of Sciences of the United States of America*, vol. 116, no. 17, pp. 8200–8205, 2019.

[23] B. Deng, P. Wang, Q. He, V. Tournat, and K. Bertoldi, "Metamaterials with amplitude gaps for elastic solitons," *Nature Communications*, vol. 9, no. 1, pp. 1–8, 2018.

[24] B. Deng, Y. Zhang, Q. He, V. Tournat, P. Wang, and K. Bertoldi, "Propagation of elastic solitons in chains of pre-deformed beams," *New Journal of Physics*, vol. 21, no. 7, 2019.

[25] J. R. Raney, N. Nadkarni, C. Daraio, D. M. Kochmann, J. A. Lewis, and K. Bertoldi, "Stable propagation of mechanical signals in soft media using stored elastic energy," *Proceedings of the National Academy of Sciences of the United States of America*, vol. 113, no. 35, pp. 9722–9727, 2016.

[26] K. Genovese, L. Lamberti, and C. Pappalettere, "Mechanical characterization of hyperelastic materials with fringe projection and optimization techniques," *Optics and Lasers in Engineering*, vol. 44, no. 5, pp. 423–442, 2006.

[27] H. L. Corrêa, A. M. F. De Sousa, and C. R. Guimarães Furtado, "Natural rubber latex: Determination and interpretation of flow curves," *Polimeros*, vol. 25, no. 4, pp. 365–370, 2015.

[28] W. V. Titow, *PVC plastics : properties, processing and applications*, 6th ed., S. S. &. B. Media, Ed. London: Science, London : Elsevier Applied, 1990.

[29] J. C. Lagarias, J. A. Reeds, M. H. Wright, and P. E. Wright, "Convergence properties of the Nelder-Mead simplex method in low dimensions," *SIAM Journal on Optimization*, vol. 9, no. 1, pp. 112–147, 1998.

[30] R. Fuhrer, C. M. Schumacher, M. Zeltner, and W. J. Stark, "Soft iron/silicon composite tubes for magnetic peristaltic pumping: Frequency-dependent pressure and volume flow," *Advanced Functional Materials*, vol. 23, no. 31, pp. 3845–3849, 2013.

[31] P. N. Kakar, J. Das, P. M. Roy, and V. Pant, "Robotic invasion of operation theatre and associated anaesthetic issues: A review," *Indian Journal of Anaesthesia*, vol. 55, no. 1, pp. 18–25, 2011.